

# *J*-matrix calculation of electron-helium *S*-wave scattering. II. Beyond the frozen-core model

Dmitry A. Konovalov

*ARC Centre for Antimatter-Matter Studies and  
Discipline of Information Technology, School of Business,  
James Cook University, Townsville, Queensland 4811, Australia*

Dmitry V. Fursa and Igor Bray

*ARC Centre for Antimatter-Matter Studies, Curtin University,  
GPO Box U1987, Perth, Western Australia 6845, Australia*

(Dated: September 7, 2012)

In the preceding *J*-matrix (JM) paper [D. A. Konovalov *et al.* Phys. Rev. A **84**, 032707 (2011)], the *S*-wave *e*-He scattering (*S*-*e*-He) problem was solved within the frozen-core (FC) model of helium for impact energies in the range 0.1-1000eV. In this sequel, both target electrons are described within the configuration-interaction model of helium obtaining more accurate (compared to the FC model) first seven bound states of the *S*-wave helium. The presented JM calculations are essentially exact numerical solution of the *S*-*e*-He problem for the total elastic,  $2^{1,3}S$ ,  $3^{1,3}S$  excitation cross sections below the ionization threshold. The JM results are confirmed by the corresponding convergent-close-coupling (CCC) calculations creating a challenging benchmark for any current or future *ab initio* electron-atom scattering methods.

Above the ionization threshold, only the elastic and triplet  $2^3S$  excitation cross sections are obtained at the benchmark accuracy level. The total ionization and the rest of excitation cross sections still exhibit noticeable pseudo-resonances (up to 10% fluctuations), which could not be eliminated with the considered number of target states (up to 95 eigenstates of He were considered).

PACS numbers: 34.80.Dp

## I. INTRODUCTION

This study focuses on the *S*-wave *e*-He (*S*-*e*-He) scattering, where the target helium atom is in its ground state before the electron impact, and where only the partial wave with zero angular momentum ( $l = 0$ ) is retained in all calculations and partial-wave expansions. The *S*-wave models have proven to be a very productive testing ground for *ab initio* scattering theories, see [1–18] for the *S*-wave *e*-H scattering (*S*-*e*-H) and [19–27] for the *S*-*e*-He problem. The main attraction of the *S*-wave models is that they retain most of the physics complexities of the full scattering problems while reduce the problems computationally. In particular, it is somewhat expected that if a theoretical method solves a *S*-wave model, then the remaining partial waves could be solved with additional computational resources, see for example the convergent-close-coupling (CCC) [28], *R*-matrix (RM) [29–31] and *J*-matrix (JM) [32, 33] methods.

The main goal of this study is to provide high accuracy total elastic and excitation *S*-*e*-He cross sections for 5-100eV impact energies highlighting resonant features of the cross sections. The need for such benchmark theoretical data is evident from the existing *ab initio* attempts to solve the *S*-*e*-He problem. Reviewing in reverse chronological order, in 2010, Bartlett and Stelbovics [25] developed a four-body propagating exterior scaling (PECS) method and reported results claiming to achieve “benchmark” level of accuracy. However none of their cross sections, including elastic and  $2^{1,3}S$  excita-

tion cross sections, displayed any resonances at the accuracy level achieved for the *S*-*e*-H problem [3]. In 2005, Horner *et al.* [24] reported results using time-dependent exterior complex scaling (TD-ECS), which also failed to described resonance behavior of the cross sections. In 2002 and 2004, the CCC method [21, 22] also did not examine the resonance regions with sufficiently fine energy grid. This is now corrected to some extent when in 2011 Konovalov *et al.* [27] reported the CCC and JM *frozen-core* (FC) results clearly showing the resonances in the elastic and  $n = 2$  ( $2^1S$  and  $2^3S$ ) excitation cross sections. And finally, the RM method [29, 31] has never reported its results for the *S*-*e*-He problem.

The stated goal is attempted and achieved in many aspects by combining advantages of the CCC and JM methods, where the later has been recently revised [27] by merging it with the Fano’s multi-configuration interaction matrix elements [34]. The CCC method is able to solve the scattering problem very accurately via the Lippmann-Schwinger equation [35]. However, it is not practical to run the CCC method for each of the many thousands of impact energy points required for the final benchmark results. On the other hand, the JM method is very efficient [36, 37] in calculating a vast number of energy points but numerical-convergence properties of the JM method remains largely unknown. The JM and CCC methods are implemented independently and use completely different approaches to solve the scattering equations. Therefore, the CCC and JM methods can be and were used to cross-verify that their results are conver-

gent within their own numerical parameters at key energy points.

The presented JM method is implemented using Java programming language, which is freely available for MS Windows, Mac OS, and many versions of Linux or Unix. See [38] for information on availability of the results and source code.

TABLE I: Energy levels [a.u.] and excitation thresholds [eV] of the first nine bound states of helium in the  $S$ -wave model.

Classification	threshold [eV]	Eigenvalues [a.u.]	$(N_c, N_t)$
He( $1s^2, ^1S$ )	0	-2.879 028 569 1	(50,50)
error =	0.001 80	-2.878 962 303	(7,30)
error =	0.015 94	-2.878 442 699	(3,30)
error =	0.177 47	-2.872 506 673	(1,30)
He( $1s2s, ^3S$ )	19.178	-2.174 264 856 3	(50,50)
		-2.174 264 618	(7,30)
		-2.174 245 504	(1,30)
He( $1s2s, ^1S$ )	19.996	-2.144 197 258 7	(50,50)
		-2.144 191 393	(7,30)
		-2.143 449 321	(1,30)
He( $1s3s, ^3S$ )	22.056	-2.068 490 070	(7,30)
		-2.068 484 660	(1,30)
He( $1s3s, ^1S$ )	22.266	-2.060 792 356	(7,30)
		-2.060 573 161	(1,30)
He( $1s4s, ^3S$ )	22.928	-2.036 438 560	(7,30)
		-2.036 436 372	(1,30)
He( $1s4s, ^1S$ )	23.011	-2.033 392 203	(7,30)
		-2.033 300 706	(1,30)
He( $1s5s, ^3S$ )	23.305	-2.022 583 695	(7,30)
		-2.022 582 608	(1,30)
He( $1s5s, ^1S$ )	23.346	-2.021 079 423	(7,30)
		-2.021 033 007	(1,30)
He $^+(1s)$	23.920	-2	Ionization

## II. THEORY

The JM method [36, 37] is a very general method for solving wide range of scattering problems. In this study, we continue to develop the version of the JM method that was previously applied to the  $S$ -e-H [39] and  $S$ -e-He [27] scattering problems. Hereafter this version will be referred to as the KFB method to assist when discussing its features which are not part of the generic JM method.

When the KFB method was applied to the FC model of helium [27] (one electron was always in the  $1s$  state of He $^+$ ), the following three sets of functions were used: target basis, JM functions, and Laguerre basis.

*Target basis* is a set of  $N_t$  orthonormal radial functions  $\{P_n(r)\}_{n=1}^{N_t}$ , where  $P_n(r)$  is used as the radial component of the  $n$ 'th subshell wave function when building one- or many-electron wave functions as per the Fano's procedure [27, 34].

*JM functions* are the nonorthogonal Laguerre func-

tions  $\{\xi_p(r)\}_{p=0}^\infty$  from the original JM method [36, 37],

$$\xi_p(r) = x^{l+1} e^{-x/2} L_p^{2l+1}(x), \quad p = 0, 1, \dots, \infty, \quad (1)$$

where  $x = \lambda r$ ,  $\lambda$  is Laguerre exponential falloff,  $l \equiv 0$  (for the  $S$ -model), and  $L_p^\alpha(x)$  are the associated Laguerre polynomials [40].

*Laguerre basis* is the set of orthonormal Laguerre functions  $\{R_p(r)\}_{p=0}^\infty$ ,

$$R_p(r) = C_p x^{l+1} e^{-x/2} L_p^{2l+2}(x), \quad p = 0, 1, \dots, \infty, \quad (2)$$

$$\int_0^\infty dr R_p(r) R_{p'}(r) = \delta_{pp'}, \quad C_p = \sqrt{\frac{\lambda p!}{(p+2l+2)!}}. \quad (3)$$

Note that for any fixed  $N_t$ , both  $\{\xi_p(r)\}_{p=0}^{N_t}$  and  $\{R_p(r)\}_{p=0}^{N_t}$  span identical functional space [39].

The target basis  $\{P_n(r)\}_{n=1}^{N_t}$  is selected or built by diagonalizing a suitable one-electron Hamiltonian [27, 39]. Then, the two-electron target-helium wave functions are constructed by allowing first and second helium electrons to occupy the first  $N_c$  and  $N_t$  radial functions, respectively, where  $N_c$  controls the number of allowed *core* excitations with  $N_c = 1$  being the frozen-core model.

After many numerical experiments, it became apparent that the core excitation functions  $\{P_n(r)\}_{n=1}^{N_c}$  should be constructed differently from the rest of the target basis  $\{P_n(r)\}_{n=N_c+1}^{N_t}$ . Otherwise, the convergence by  $N_c$  is just too slow to be computationally practical. This is due to the two very different radial scales present in this study. The short-range core excitations are essentially adjustments to the  $1s$ -orbital of He $^+$ . While the helium excitations below the ionization threshold resemble  $ns$ -orbitals of hydrogen and therefore are long-range. This problem is solved here by using a mix of the short range  $\{R_p^c(r)\}_{p=0}^{N_c-1}$  with  $\lambda_c = 4$  and long-range  $\{R_p^t(r)\}_{p=N_c}^{N_t-1}$  with  $\lambda_t = 1$  basis sets when constructing the target basis as follows.

The JM method splits the one-electron radial functional space into *inner*  $\{\xi_p\}_{p=0}^{N_t-1}$  and *outer*  $\{\xi_p\}_{p=N}^\infty$  subsets controlled by the number  $N$  of JM functions in the inner subset [36, 37]. In the KFB method, the target basis  $\{P_n(r)\}_{n=1}^{N_t}$  must be orthogonal to the outer JM functions  $\{\xi_p\}_{p=N}^\infty$ , where  $N_t < N$ . Let  $\lambda \equiv \lambda_t$  and  $\hat{I}_t$  be a projection operator into the functional space of  $\{R_p^t(r)\}_{p=0}^{N_t-1}$

$$\hat{I}_t = \sum_{p=0}^{N_t-1} |R_p^t\rangle \langle R_p^t|, \quad (4)$$

then by construction every function from  $\{R_p^t(r)\}_{p=0}^{N_t-1}$  and  $\{R_p^c(r)\}_{p=0}^{N_c-1}$

$$R_p^{ct} = \hat{I}_t R_p^c, \quad (5)$$

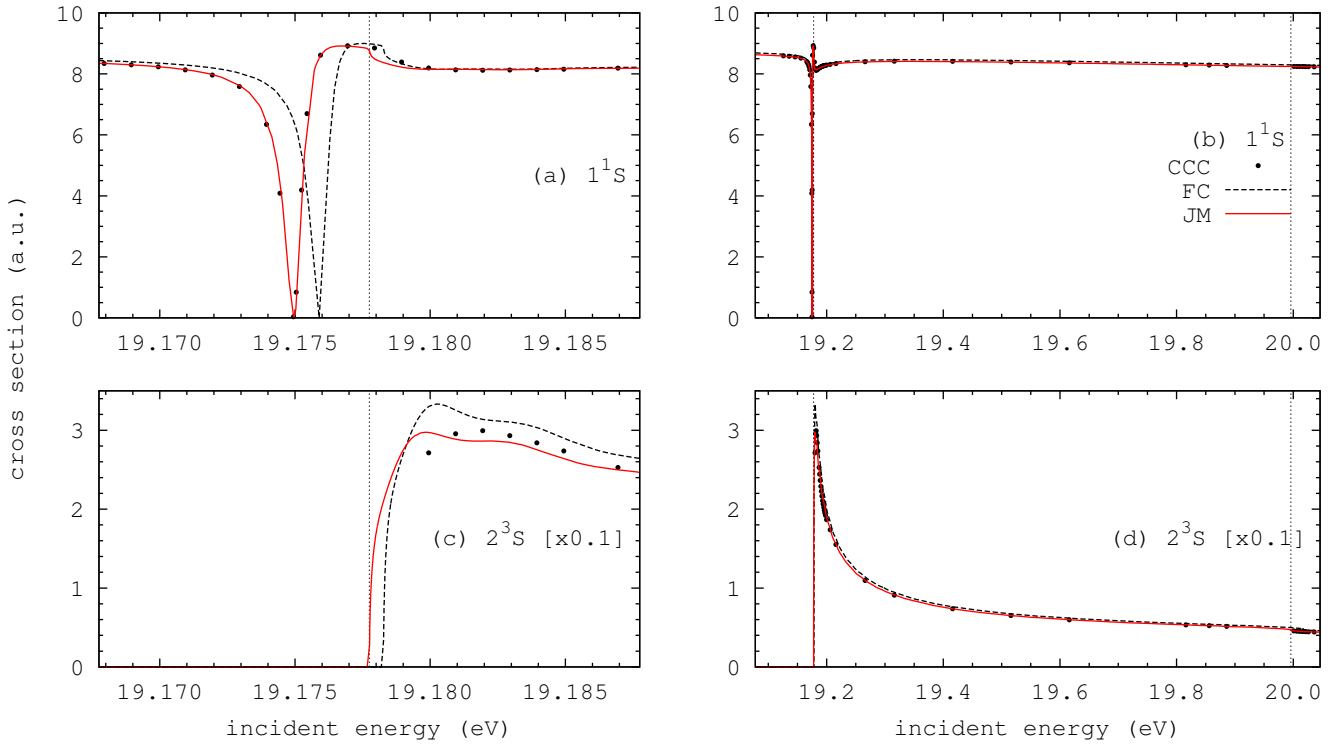


FIG. 1: (Color online) Elastic ( $1^1S$ ) and  $2^3S$  single-excitation  $e$ -He  $S$ -wave cross sections between and around  $2^3S$  and  $1^1S$  thresholds shown by vertical dashed lines. Sub-figures (a) and (c) zoom in on the  $2^3S$  excitation threshold (Table I). FC (Frozen-core,  $N_c = 1$ ,  $N_t = 30$ ), JM ( $N_c = 7$ ,  $N_t = 30$ ) and CCC ( $N_c = 3$ ,  $N_t = 30$ ) results were shifted to the right by 0.17747eV, 0.0018eV and 0.01594eV (Table I), respectively.

is orthogonal the outer JM functions. The final target basis  $\{P_n(r)\}_{n=1}^{N_t}$  is constructed by making a single orthonormal basis from  $\{R_p^{ct}(r)\}_{p=0}^{N_c-1}$  and  $\{R_p^t(r)\}_{p=N_c}^{N_t-1}$  via the Gram-Schmidt process.

Note that in the CCC method the final target basis  $\{P_n^{3c}(r)\}_{n=1}^{N_t}$  is also built via the Gram-Schmidt process but from  $\{R_p^c(r)\}_{p=0}^{N_c-1}$  and  $\{R_p^t(r)\}_{p=N_c}^{N_t-1}$  sets, that is, the intermediate  $R_p^{ct}$  functions were not required.

### III. RESULTS AND DISCUSSION

See Supplemental Material at [URL will be inserted by publisher] for the results in tabular form.

The number  $N$  is the key JM parameter responsible for the convergence of any implementation of the JM method. That is, the larger the  $N$ , the more accurate the corresponding JM results are expected to be. Within the current KFB method, maximum value of  $N$  is limited to around 100 so that the method remains to be easily accessible to wider research community. All presented in this study KFB results were still calculated on a consumer-grade laptop.

The following KFB computational parameters were used, see [39] for explanation of the parameters:  $\lambda_c = 4$ ,  $\lambda_t = 1$ ,  $N_t = 30$ ,  $N = 100$ ,  $\ln(c) = -5 - 2\ln(Z_{\text{He}})$ ,

$Z_{\text{He}} = 2$ ,  $r_{\text{max}} = 500$ ,  $M_{LCR} = 2001$ , where the radial grid was between zero and  $r_{\text{max}}$ , and  $M_{LCR}$  is the number of equally spaced points in the radial LCR grid [39]. Hereafter FC, JM and CCC denote results obtained with  $N_c = 1$ ,  $N_c = 7$  and  $N_c = 3$ , respectively. The ( $N_c = 7$ ,  $N_t = 30$ ,  $N = 100$ )-combination yields 51 singlet ( $1^1S$ ) and 44 triplet ( $3^1S$ ) eigenstates of helium, and 8418 eigenstates of  $\text{He}^-(2^3S)$ . When converting to eV scale, 27.2116 eV was used as the atomic unit of energy (or Hartree).

Table I shows first nine eigenvalues from diagonalizations of  $S$ -wave helium Hamiltonian. Selecting  $\lambda_c = 4$  creates the first target radial function  $P_1(r)$  numerically identical to the exact  $1s$  state of  $\text{He}^+$ , when  $N_t$  is sufficiently large as is the case for the used  $N_t = 30$ . The main improvement of the  $N_c = 7$  basis over the frozen-core case ( $N_c = 1$ ) is in the ground state of helium, where the first seven significant figures [41] were obtained by using  $\{R_p^c(r)\}_{p=0}^{N_c-1}$  as the basis for both electrons with  $N_c = 50$  and  $\lambda_c = 4$ , denoted by (50, 50) in Table I.

Fig. 1 shows that if the FC results are shifted (as they are on all the figures) to the right by the FC ground energy error (0.17747eV, see Table I), the FC and JM results become very close. This means that most of the  $S$ -wave scattering dynamics is essentially due to the movement of one electron in the field of  $1s$  state of  $\text{He}^+$ . Fig. 1(b) zooms in onto the negative-ion resonance  $\text{He}^-(1s2s^2, ^2S)$  that exists [42] just below the  $2^3S$ -

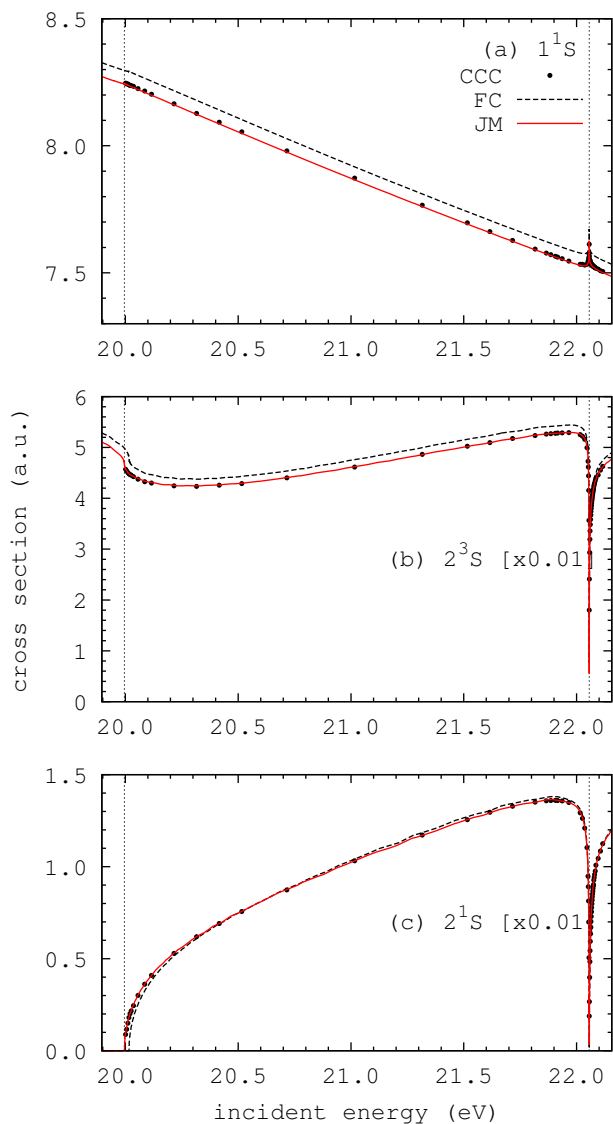


FIG. 2: (Color online) The same as in Fig. 1 with added  $2^1S$  excitation cross section for incident energies between and around  $2^1S$  and  $3^3S$  thresholds shown by vertical dashed lines.

excitation threshold. Here the full JM results are still qualitatively similar to the FC results.

Threshold behavior is examined in Fig. 3, where only the triplet excitation cross sections exhibit sharp resonance peaks immediately above the thresholds. This is very different from the full (all  $L$ 's)  $e$ -He scattering problem, where the singlet cross sections have the resonance peaks just above the thresholds [30, 43]. Fig. 3 illustrates how additional angular momenta (mainly  $P$ -wave) could shift the corresponding negative-ion states below the triplet excitation and create new  $\text{He}^-$  states just above the singlet thresholds [30, 31].

Fig. 4 shows the rich interplay of cross sections at the same energies. In particular, the  $\text{He}^-(^2S)$  resonances exist just the triplet helium states, where they become broader (smaller amplitude of pick) from  $4^3S$  to  $7^3S$  after which they are no longer detectable.

#### IV. CONCLUSIONS

We have applied the JM method to the

#### Acknowledgments

This work was supported by the Australian Research Council. IB acknowledges the Australian National Computational Infrastructure Facility and its Western Australian node iVEC.

- 
- [1] A. Temkin, Phys. Rev. **126**, 130 (1962).
  - [2] E. J. Heller and H. A. Yamani, Phys. Rev. A **9**, 1209 (1974).
  - [3] R. Poet, J. Phys. B **11**, 3081 (1978).
  - [4] R. Poet, J. Phys. B **13**, 2995 (1980).
  - [5] R. Poet, J. Phys. B **14**, 91 (1981).
  - [6] J. Callaway and D. H. Oza, Phys. Rev. A **29**, 2416 (1984).
  - [7] I. Bray and A. T. Stelbovics, Phys. Rev. Lett. **69**, 53 (1992).
  - [8] A. K. Bhatia, B. I. Schneider, and A. Temkin, Phys. Rev. Lett. **70**, 1936 (1993).
  - [9] D. A. Konovalov and I. E. McCarthy, J. Phys. B **27**, L407 (1994).
  - [10] W. Ihra, M. Draeger, G. Handke, and H. Friedrich, Phys. Rev. A **52**, 3752 (1995).
  - [11] M. S. Pindzola and D. R. Schultz, Phys. Rev. A **53**, 1525 (1996).
  - [12] S. Jones and A. T. Stelbovics, Phys. Rev. A **66**, 032717 (2002).
  - [13] S. Jones and A. T. Stelbovics, Phys. Rev. Lett. **84**, 1878 (2000).
  - [14] M. Baertschy, T. N. Rescigno, W. A. Isaacs, and C. W. McCurdy, Phys. Rev. A **60**, R13 (1999).
  - [15] A. T. Stelbovics, Phys. Rev. Lett. **83**, 1570 (1999).
  - [16] C. W. McCurdy, D. A. Horner, and T. N. Rescigno, Phys. Rev. A **65**, 042714 (2002).
  - [17] P. L. Bartlett and A. T. Stelbovics, Phys. Rev. A **69**, 022703 (2004).

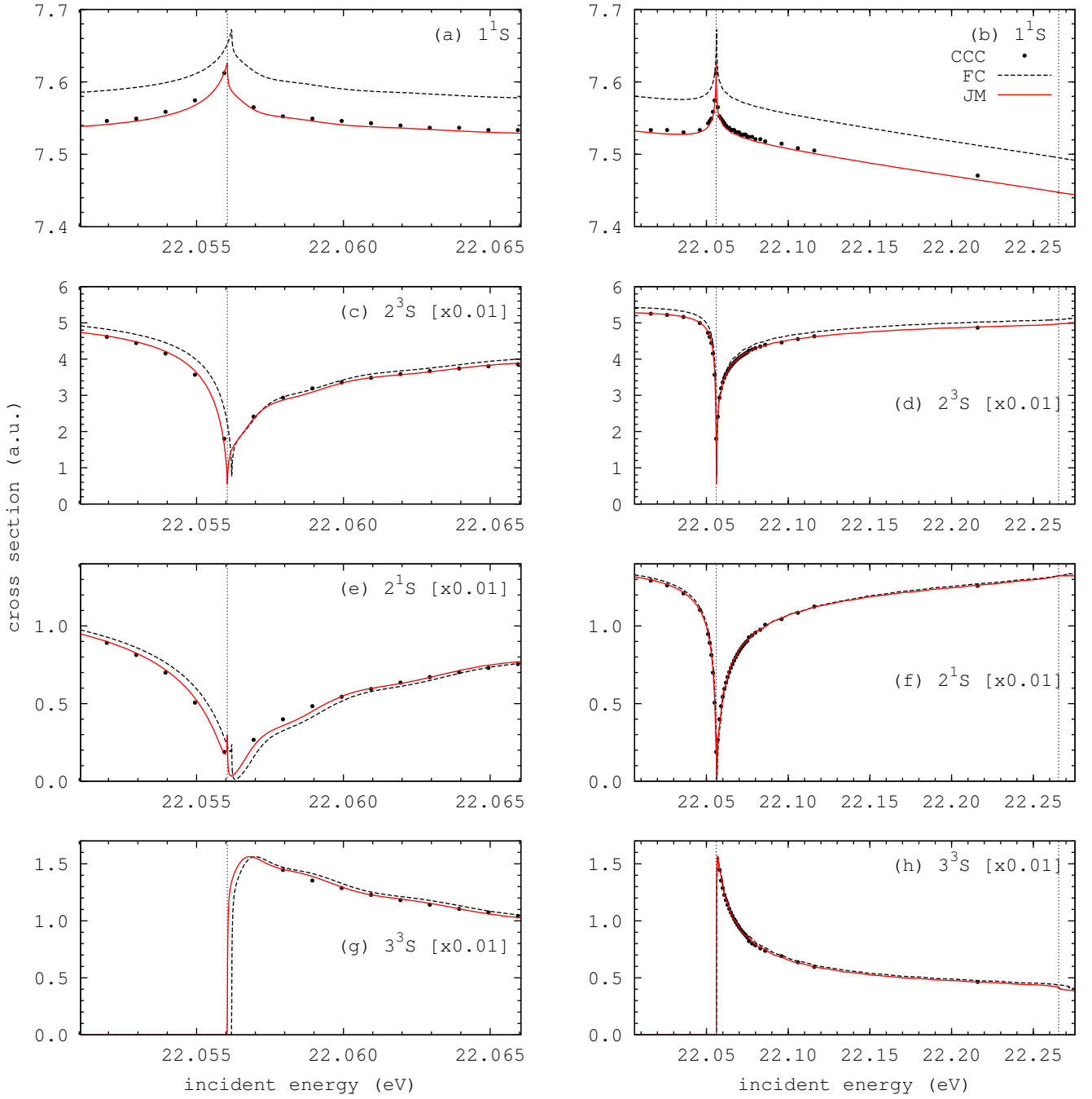


FIG. 3: (Color online) The same as in Fig. 2 with added  $3^3S$  excitation cross section between and around the  $3^3S$  and  $3^1S$  thresholds shown by vertical dashed lines. Sub-figures (a), (c), (e) and (g) zoom in on the  $3^3S$  excitation threshold (Table I).

- [18] A. L. Frapiccini, J. M. Randazzo, G. Gasaneo, and F. D. Colavecchia, J. Phys. B **43**, 101001 (2010).
- [19] M. Draeger, G. Handke, W. Ihra, and H. Friedrich, Phys. Rev. A **50**, 3793 (1994).
- [20] M. S. Pindzola, D. Mitnik, and F. Robicheaux, Phys. Rev. A **59**, 4390 (1999).
- [21] C. Plottke, I. Bray, D. V. Fursa, and A. T. Stelbovics, Phys. Rev. A **65**, 032701 (2002).
- [22] C. Plottke, P. Nicol, I. Bray, D. V. Fursa, and A. T. Stelbovics, J. Phys. B **37**, 3711 (2004).
- [23] D. A. Horner, C. W. McCurdy, and T. N. Rescigno, Phys. Rev. A **71**, 010701(R) (2005).
- [24] D. A. Horner, C. W. McCurdy, and T. N. Rescigno, Phys. Rev. A **71**, 012701 (2005).
- [25] P. L. Bartlett and A. T. Stelbovics, Phys. Rev. A **81**, 022715 (2010).
- [26] P. L. Bartlett and A. T. Stelbovics, Phys. Rev. A **81**, 022716 (2010).
- [27] D. A. Konovalov, D. V. Fursa, and I. Bray, Phys. Rev. A **84**, 032707 (2011).

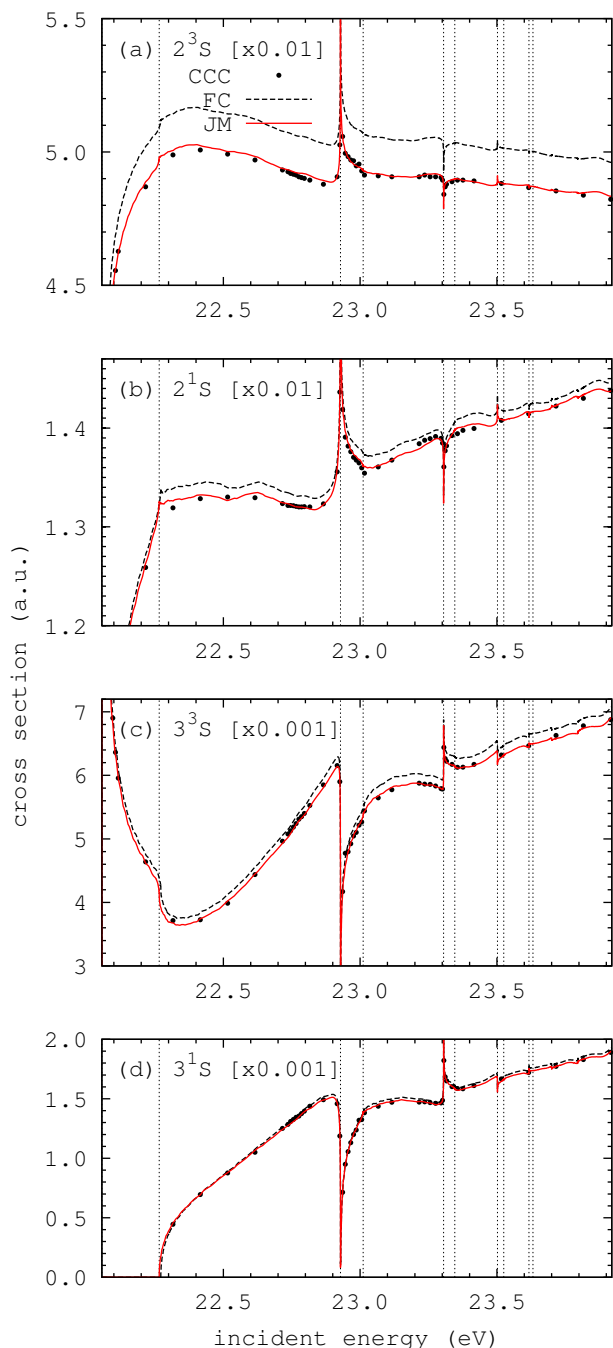


FIG. 4: (Color online) The same as in Fig. 3 with added  $3^1S$  excitation cross section between the  $3^3S$  and ionization thresholds (23.92eV, Table I). The  $3^1S$ ,  $4^{3,1}S$ , ...,  $7^{3,1}S$  excitation thresholds (Table I) are shown by vertical dashed lines (from left to right).

- [28] D. V. Fursa and I. Bray, Phys. Rev. A **52**, 1279 (1995).
- [29] W. C. Fon, K. P. Lim, K. Ratnavelu, and P. M. J. Sawey, Phys. Rev. A **50**, 4802 (1994).
- [30] K. Bartschat, E. T. Hudson, M. P. Scott, P. G. Burke, and V. M. Burke, Phys. Rev. A **54**, R998 (1996).
- [31] M. Stepanovic, M. Minic, D. Cvejanovic, J. Jurata, J. Kurepa, S. Cvejanovic, O. Zatsarinny, and K. Bartschat, J. Phys. B **39**, 1547 (2006).
- [32] D. A. Konovalov and I. E. McCarthy, J. Phys. B **27**, L741 (1994).
- [33] D. A. Konovalov and I. E. McCarthy, J. Phys. B **28**, L139 (1995).
- [34] U. Fano, Phys. Rev. **140**, A67 (1965).
- [35] I. Bray and A. T. Stelbovics, Phys. Rev. A **46**, 6995 (1992).
- [36] E. J. Heller and H. A. Yamani, Phys. Rev. A **9**, 1201 (1974).
- [37] J. Broad and W. Reinhardt, J. Phys. B **9**, 1491 (1976).
- [38] The complete Java source code used in this study is freely available for academic use from [jmatrix.googlecode.com](http://jmatrix.googlecode.com) or a relevant link at [www.dmitrykonovalov.org](http://www.dmitrykonovalov.org).
- [39] D. A. Konovalov and I. Bray, Phys. Rev. A **82**, 022708 (2010).
- [40] M. Abramowitz and I. A. Stegun, eds., *Handbook of Mathematical Functions* (Dover Publications, Mineola, NY, 1965).
- [41] S. P. Goldman, Phys. Rev. Lett. **73**, 2547 (1994).
- [42] S. J. Buckman and C. W. Clark, Rev. Mod. Phys. **66**, 539 (1994).
- [43] R. K. Nesbet, Phys. Rev. A **12**, 444 (1975).

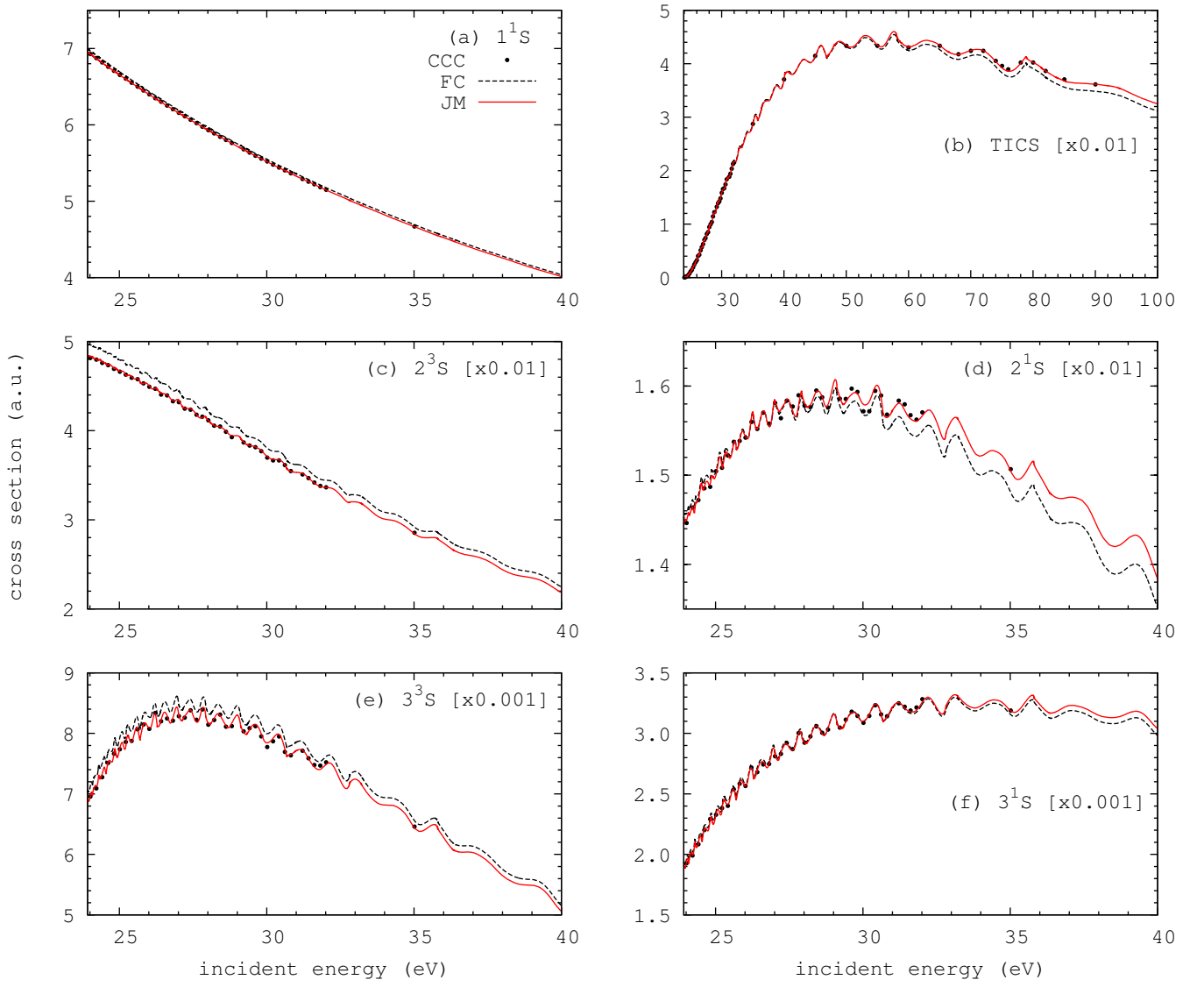


FIG. 5: (Color online) The same as in Fig. 4 with added total ionization cross section (TICS) for incident energies above ionization threshold.